Published as: Walter W Focke, Washington Mhike, Herman J Kruger, Riaan Van Schalkwyk, Dewan Lombaard, Heinrich Badenhorst. Commercial Expandable Graphite Flame Retardants. Thermochimica Acta 584 (2014) 8–16.
http://dx.doi.org/10.1016/j.tca.2014.03.021

Characterization of commercial expandable graphite fire retardants

Walter Wilhelm Focke, Heinrich Badenhorst, Washington Mhike, Hermanus Joachim Kruger, Dewan Lombaard

SARChI Chair in Carbon Technology and Materials, Institute of Applied Materials, Department of Chemical Engineering, University of Pretoria, Private Bag X20, Hatfield 0028, South Africa

Abstract

Thermal analysis and other techniques were employed to characterize two expandable graphite samples. The expansion onset temperatures of the expandable graphite's were ca. 220 °C and 300 °C respectively. The key finding is that the commercial products are not just pure graphite intercalation compounds with sulfuric acid species intercalated as guest ions and molecules in between intact graphene layers. A more realistic model is proposed where graphite oxide-like layers are also randomly interstratified in the graphite flakes. These graphite oxide-like layers comprise highly oxidized graphene sheets which contain many different oxygen-containing functional groups. This model explains the high oxygen to sulfur atomic ratios found in both elemental analysis of the neat materials and in the gas generated during the main exfoliation event.

Keywords: Expandable graphite; graphite oxide; graphite intercalation compound; exfoliation; thermal analysis

---

*Corresponding author: Tel: +27 12 420 3728. Fax: +27 12 420 2516. E-mail address: walter.focke@up.ac.za (W.W. Focke)

1. Introduction

Natural flake graphite (FG) is a layered mineral made up of stacked graphene sheets of covalently bonded carbon atoms [1, 2]. Due to the anisotropic nature of graphite it possesses high but non-uniform electrical conductivity. It is high in the in-plane direction but much lower in the direction perpendicular to the graphene layers [1].

Graphite oxide (GO) is a highly oxidized and disordered form of graphite that contains carbon, oxygen, and hydrogen in variable ratios [1, 3-5]. It is synthesized by exposing flake graphite to concentrated sulfuric acid in conjunction with strong oxidizers such as nitric acid or potassium permanganate [3, 4]. Mermoux and Chabre [6] contend that GO is obtained via hydrolysis of an intermediary compound formed through over-oxidation of a graphite intercalation compound. Graphite oxide retains the lamellar structure of the parent graphite but with a much larger and irregular basal spacing (d_{002} between 0.562 nm and 0.902 nm [7]) owing to the presence of oxygen-containing groups [3]. The nature of GO is not well defined but it is believed that it has enol, keto and epoxy functional groups randomly attached to the graphene sheets [5]. Depending on the synthesis method, the oxygen content can range from 44 wt.% to 56 wt.% and the carbon to oxygen ratio from about 1.0 to 1.6 [3, 4]. Owing to the highly oxidized nature of the graphene sheets, GO is an insulator material [1].

Graphite intercalation compounds (GICs) possess guest molecules inserted (intercalated) between the graphite layers [8]. The graphite layers in these complex materials remain largely intact with the guest molecules or atoms (X) located in between graphene layers. The actual composition varies on a layer by layer basis as not every layer becomes intercalated. This phenomenon is called staging and a stage *n* compound will have *n* graphite layers with no guests in between them for each intercalated layer. In other words, the stage number *n* is simply the number of graphene layers sandwiched between successive intercalant layers. This

means that in a stage 1 (or first stage) compound the graphite layers and intercalant layers alternate perfectly. Such compounds may be described by the formula XC_y.

Graphite bisulfate is a stage 1 lamellar compound (d-spacing of 0.397 nm) which possesses a blue hue [9, 10]. The composition of the Stage 1 compound is stated as $C_{24}^{+}\cdot HSO_4^{-}\cdot 2H_2SO_4$ [11, 12]. Graphite bisulfate may be produced electrochemically [11] or by dipping natural graphite in concentrated sulfuric acid with sufficient nitric acid to oxidise the graphite to prepare it for intercalation [9]. Graphite bisulfate is, however, highly unstable and decomposes if a small amount of water is added to the acid or if the blue compound is exposed to air. One may observe the breakdown of graphite bisulfate exposed to moist air over time by following the change in its XRD patterns. Ultimately, breakdown of graphite bisulfate results in a residue with a very broad XRD reflection at a d-spacing of 0.339 nm [9]. It appears to be a mixture of various higher stages of sulphuric acid intercalated graphite. Hennig [13] suggested that the composition of the degraded residue can be approximated by $C_n^{+}\cdot HSO_4^{-}\cdot 4H_2SO_4$ with impurities distributed in a state of high disorder.

Industrial-scale synthesis of expandable graphite (EG) utilizes liquid-phase graphite – sulfuric acid reactions in the presence of strong chemical oxidants such as $KMnO_4$, HNO_3 and H_2O_2 [14]. At this scale it is, in effect, produced in a similar fashion to graphite oxide. The parallels between the production methods for graphite oxide and graphite bisulfate imply the possibility that both compounds may be formed during expandable graphite production. According to Camino et al. [15], expandable graphite is equivalent to a staged version of a graphite-sulfuric acid salt, i.e. the graphene layers all remain intact while bisulfate ions are intercalated between these layers. Talanov et al., however, [16] suggests that expandable graphite is obtained via hydrolysis of graphite bisulfate, implying that is a less well-ordered material than its graphite bisulfate progenitor.

The key property of expandable graphite is its tendency to exfoliate when heated to high temperatures beyond a characteristic expansion onset temperature. During exfoliation it expands rapidly in a worm-like manner to form vermicular graphite with a low density [1, 2, 17]. The exfoliation process is an endothermic event and the expansion follows ideal gas law behaviour. According to Chung [17] the origin of this process lies in the vaporization of the intercalant.

Expandable graphite and its exfoliated form may be used in numerous applications [17]. These include gaskets; seals and packings; fire extinguisher agents; thermal insulators; electrodes; for the production of high thermal conductivity graphite sheets; etc. [17]. Expandable graphite may act as a intumescent flame retardant for some polymers [18-23] with polyethylene [24] and polyurethane foams being the primary substrates for EG [15, 21]. Expandable graphite possess similar in-plane electrical conductivity to natural flake graphite [25]. This means that it could impart both antistatic and thermal conductivity [26] in addition to flame retardant properties to polymers [27]. Natural graphite and expandable graphite therefor possess the ability to impart both electrical and thermal conductivity into its polymer substrate while improving fire retardancy properties in addition to the aforementioned effects. This investigation and its associated projects aim to explore the use of these additives in a variety of applications ranging from flame retardants to heat storage materials [27-30]. The objective of this particular study in particular was to perform a comprehensive characterization of two commercial expandable graphite grades used in industrial polymer applications. The aim was to gain a better understanding of the true nature of expandable graphite grades used in industry. Finally, this communication complements previous studies that have investigated the thermal properties of graphite bisulphate [11, 31].

2. Experimental

2.1 Materials

Two grades of expandable graphite, ES 250 B5 (onset temperature 220°C) and ES170 300A (onset temperature 300°C), were obtained from Qingdao Kropfmuehl Graphite (China). Milled natural Zimbabwean flake graphite (Graphite) was supplied by BEP Bestobell (South Africa). Exfoliated graphite forms were prepared at a temperature of 600 °C by placing the expandable graphite powder samples in a Thermopower electric furnace.

2.2 Particle size, BET surface and density determination

The graphite particle size distributions were determined with a Mastersizer Hydrosizer 2000MY (Malvern Instruments, Malvern, UK). The specific surface areas of the graphite powders were determined BET surface areas were measured on a Micromeritics Flowsorb II 2300 and a Nova 1000e BET instrument in N_2 at 77 K. Densities were determined on a Micrometrics AccuPyc II 1340 helium gas pycnometer.

2.3 Thermogravimetry (TGA)

Thermogravimetric analysis (TGA) was performed using the dynamic method on a Mettler Toledo A851 TGA/SDTA instrument. About 5 mg powder was placed in an open 150 µL alumina pan. Temperature was scanned from 25 to 1000 °C at a scan rate of 10 °C/min with air or N_2 flowing at a rate of 50 mL/min

2.4 Composition of evolved gases

Approximately 50 g samples of expandable graphite were placed in a graphite crucible. They were heated in a Thermal Technologies high temperature graphitizing furnace. The temperature was ramped up at a rate of 1 °C/min starting from 100 °C and ending at 600 °C. Helium was passed through the furnace at a flow rate of 0.1 L/min. A Teledyne PEM9004

portable emissions analyser was used to determine the concentration of SO_2 in the flue gas stream as a function of temperature.

The overall composition of the gases evolved during exfoliation was determined as follows. Approximately 3 g samples of expandable graphite were placed in a sealed reaction vessel in a Thermopower furnace. The temperature was ramped up at a rate of 5 °C/min starting from 100 °C and ending at 600 °C. A sample gas bag was connected to the reactor purge line. The gases emitted from the process were trapped in SKC Flexifilm gas bags. Gas analysis was performed using gas chromatography by a SANAS accredited laboratory.

2.5 Graphite composition determinations

Elemental analysis was performed on a Thermo Scientific Flash 2000 CHNS Elemental Analyser with the furnace temperature set at 900 °C. The sulphur content was also checked using an Eltra CS-580 analyser.

The elemental composition of the inorganic part of the graphite powders was also measured using XRF analysis performed using a wavelength-dispersive spectrometer (ARL 9400XP+ XRF). The samples were prepared as pressed powder briquettes and introduced to the spectrometer. The powders were also ground in a tungsten carbide milling vessel and roasted at 1000°C for determination of the loss on ignition (LOI).

2.6 Ion exchange

EG grade ES250 B5 (43.2 g) was successively suspended in fresh portions of ca. 150 g of 27.4 wt.% diammonium phosphate (DAP) solution. The suspension was left to stand for one day before the expandable graphite was separated by filtration for further suspension in a fresh portion of the DAP solution. This procedure was repeated four times. After the final

treatment, the graphite was thoroughly washed with deionized water. The recovered liquid filtrates and wash water were analysed for sulfate and phosphate to determine the amount of sulfate ions exchanged and the quantity of phosphate ions intercalated.

2.7 Thermomechanical analysis

Thermal expansion measurements were conducted on a TA instruments Q400 Thermo Mechanical Analyser. Sufficient powder was placed in an alumina sample pan such that the bed height was between 35 μm and 40 μm. The flake expansion behaviour was measured with a flat-tipped standard expansion probe using an applied force of 0.02 N. The temperature was scanned from 30 °C to 1000 °C at a scan rate of 10 °C/min in nitrogen atmosphere. The expansion relative to the original powder bed height was reported.

2.8 X-Ray Diffraction (XRD)

XRD diffraction patterns were recorded using a Bruker D8 Advance powder diffractometer fitted with a Lynx eye detector. Measurements were performed in the 2θ range 15-120 ° with a 0.04 ° step size and a counting time of 0.2 s. The interlayer spacing, d_{002}, was calculated using the Bragg equation, was used as an indicator for the extent of ordering.

2.9 Raman spectroscopy

The Raman spectra were recorded with a T64000 series II triple spectrometer system from HORIBA Scientific, Jobin Yvon Technology using the 514.3 nm laser line of a coherent Innova®70 Ar^+ laser with a resolution of 2 cm^{-1} in the range 1200 to 1700 cm^{-1}. The samples were recorded in a backscattering configuration with an Olympus microscope attached to the instrument (using a LD 50x objective). The laser power was set at of 6 mW and a nitrogen-

cooled CCD detector was used. The accumulation time was 120 s and the spectra were baseline corrected with using LabSpec software.

2.10 Scanning Electron Microscopy (SEM)

Graphite morphologies were studied using an ultrahigh resolution field emission scanning electron microscope (HR FEGSEM Zeiss Ultra Plus 55) with an InLens detector at an acceleration voltage of 1 kV to ensure maximum resolution of surface detail. No electrically-conductive coating was applied to the graphite particles. Microanalysis was performed with a Thermo Scientific NanoTrace X-ray detector. This analysis was performed with the microscope magnification at 750× and an accelerating voltage of 20 kV.

3. Results

3.1 Graphite particle characteristics

Figure 1 shows the particle size distribution of the various graphite types used. The d_{50} particle size of the natural flake graphite was almost five times lower than that of the two expandable graphite grades. The d_{10}, d_{50}, and d_{90} particle sizes, BET surface area, and densities of the different graphite samples are presented in Table 1. The surface area of the ES170 300A expandable graphite samples increased by a factor of twenty two when it expanded during heat treatment at 600 °C. The surface area of the neat ES250 B5 could not be determined as it started to exfoliate during BET measurement attempts. Figure 2 indicates the flake-like nature of the natural and expandable graphite. The expanded graphite samples in Figure 2 have worm-shaped, accordion-like structures. Slit-shaped gaps between the graphite platelets are clearly visible in the high resolution micrographs.

The microstructures of the expanded worms are built up of distorted graphite sheets. It is possible to consider these worms to be comprised of several discrete flake remnants with a

thickness distribution. Owing to their very high aspect ratios, the average thickness of these sheets can be estimated from the BET surface area using the equation

$$t = 2/\rho A \quad (1)$$

Where t is the average sheet thickness in m, ρ is the density in kg m^{-3}; and A is the BET surface area in m^2 kg^{-1}. Note that equation (1) neglects the edge surface area of the flakes. Applying this equation to the expanded graphite samples yields average flake thicknesses of 40 nm and 60 nm for ES250 B5 and ES170 300A respectively. This confirms the nanostructured nature of the expanded "worms".

3.2 Thermogravimetry (TGA)

Figure 3 shows the TGA mass loss curves for the expandable graphite samples in nitrogen. The exfoliation of the ES250 B5 grade occurs in two steps. Expansion onset occurs at 190 °C and the DTG peaks (not shown) occur at 205 °C and 407 °C. In contrast, the ES170 300A TGA trace indicates a single-step exfoliation event with an onset temperature above 250 °C and a DTG peak at 296 °C in the TGA. At 600 °C the ES250 and the ES170 samples have lost 15.3 wt.% and 7.3 wt.% respectively. At higher temperatures all samples oxidized and rapidly lose mass. However, there are significant differences in the oxidative stability. The thermal stability increased in the order ES250 < ES170 < natural graphite.

3.3 Composition of evolved gases

Camino et al. [15] postulated that a redox reaction between the H_2SO_4 and graphite generates the blowing gases in expandable graphite:

$C + 2H_2SO_4 \rightarrow CO_2 + 2H_2O + 2SO_2$

Scheme I. Redox reaction postulated by Camino et al. [15] for the blowing gases responsible for the exfoliation of expandable graphite.

Indeed, Figure 4 shows that SO_2 is evolved during the exfoliation of expandable graphite samples in the graphitizing furnace. Note that the onset temperature for SO_2 release was lower for ES250 than for ES170. The latter also released significantly less SO_2 during exfoliation.

Table 2 gives the overall composition of the gases collected during these experiments. They were collected in the temperature interval 100 °C to 600 °C. Table 2 also reports selected atomic ratios. The main constituents in order of decreasing importance are carbon dioxide > carbon monoxide > sulphur dioxide. This observation does not agree with the reaction mechanism posed in Scheme I which suggests that two mole SO_2 should be released for every mole of CO_2. Furthermore, if the graphite samples only contained intercalated sulphate ions, the expected oxygen to sulphur ratio would be four. However, the observed ratios are much higher, twenty seven times for ES250 and three times higher for ES170.

3.4 Graphite composition determinations

Table 3 reports the elemental analysis results and Table 4 the XRF data. Note that the sulfur content of ES250 B5 is higher than that of ES170 300A. The interesting observations are that a significant percentage of the sulfur is retained and that the carbon content increased following exfoliation at 600 °C. The data also indicate that the expandable graphite contained significant amounts of oxygen. Indeed the elemental analysis indicates oxygen contents of 12.3 wt.% and 8.4 wt.% for ES250 and ES170 respectively! Following exfoliation at 600 °C

the oxygen contents of the residues is significantly lower, i.e. 2.2 wt.% and 2.3 wt.% respectively.

Detailed examination of the elemental analysis data in combination with the TGA data indicate that 85% and 75% of the oxygen, initially present, volatilized during the exfoliation of respectively the ES250 and ES170 EG's up to 600 °C. Considering the composition of the evolved gases and using the amounts of oxygen as the link, total mass losses of 14.8 wt.% and 10 wt.% were calculated for the exfoliation process. Considering the scatter in the experimental data, this compares favourably with the actual mass losses recorded in the TGA experiments (15.3 wt.% and 7.3 wt.% for ES250 and ES170 respectively).

The sulfur content of ES250 B5 (4.0 wt.%) translates into 12.1 wt.% SO_4 assuming that all of the sulfur is initially present as sulfate. Repeated washing with deionized water recovered 1.6 wt.% sulfate while the exhaustive ion exchange experiment removed 8.4 wt.% sulfate and replaced it with DAP in the expandable graphite. This indicates that most of the sulfur is indeed present as exchangeable sulfate ions consistent with sulfate intercalated graphite.

EDS analysis confirmed the presence of sulfur in both the neat and the exfoliated expandable graphite samples. However, in the latter case the sulfur was strongly associated with calcium. This suggests the formation of calcium sulfate or sulfide during the exfoliation process and explains why part of the sulfur is retained. However, the concentration of alkali and alkaline earth metals found by XRF was too low to explain the retention of all of the sulfur in the form of sulfate or sulfide salts. This means that sulfur must also be retained in the graphite matrix, perhaps acting as sulfide bridges that neutralize dangling carbon bonds at holes and the edges of graphene sheets. Furdin [32] postulated that some of the sulfur might even be retained in its elemental form.

XRF results revealed that the inorganic content of the Zimbabwean flake graphite was about 8 wt.%. The main impurities appeared to be silica and clay minerals. According to the XRF

results, the apparent carbon content of the two expandable graphite samples were both about 89 wt.%. These values are higher than those obtained from the elemental analysis most likely because this value did not take into account the oxidized nature of the graphite samples.

The XRF results provide hints regarding the way the two expandable graphite samples were made. Unlike ES170, ES250 contains manganese and potassium suggesting the $KMnO_4$ was used as oxidant in its manufacture.

3.5 Thermomechanical analysis

A key property of expandable graphite is the ability to exfoliate over a narrow temperature range. Figure 5 shows the expansion behaviour of the graphite samples as characterized by TMA. The onset temperatures for the ES250 and ES170 were about 225 °C and 300 °C respectively. The ES250 showed a greater expansion most likely due to the larger volume of gas released by this grade during the exfoliation event.

3.6 X-Ray Diffraction (XRD)

Figure 6 shows XRD diffractograms for the two expandable graphite samples and compares them to the diffractogram for the natural graphite. Table 5 lists the d-spacing calculated from the positions of the main reflections observed in the diffractograms. The d-spacing for the natural graphite was 0.335 nm. The diffractograms of both expandable graphite samples in their neat and their expanded forms showed a peak (or at least a shoulder) that corresponded approximately to the same d-spacing. This is evidence for at most partial sulphate intercalation, i.e. the flakes also contain unreacted graphite layers. The neat expandable graphite samples featured an additional reflection located at a slightly lower angle. This corresponds to the sulphuric acid intercalated graphite phase. Comparing the reflections in the two diffractograms suggests that this phase has a higher prevalence in ES250 than in

ES170. After exfoliation, the reflections associated with this phase disappear completely and only a pure graphite reflection is evident.

The XRD pattern for ES250 features another very broad reflection with a peak at $2\theta = 15.91°$ corresponding to a d-spacing of 0.65 nm. A similar reflection occurs in the XRD pattern for ES170. It is located at $2\theta = 16.90°$ corresponding to a d-spacing of 0.61 nm. The broad nature of these reflection and their peak locations are consistent with the presence of a graphite oxide phase.

3.7 Raman spectroscopy

Figure 7 shows Raman spectra. The Raman spectrum of the natural exhibits a characteristic strong G band at 1580 cm^{-1} which is attributed to the vibration of sp^2-bonded carbon atoms in the two-dimensional hexagonal lattice. It also features a weak D band at 1349 cm^{-1} which is caused by the graphite edges or by imperfections. The Raman spectra of the expandable graphite samples exhibit a typical graphite-like pattern (Figure 7). Table 5 reports the I_D/I_G peak intensity ratios for the natural graphite and the neat as well as exfoliated expandable graphite samples. Lower values for this ratio indicate increased ordering [33]. Thus the apparent ordering of the graphite improves on exfoliation. Botas [34] reported peak intensity ratios for graphite oxide of $I_D/I_G \approx 0.9$. This indicates that the disorder in the expandable graphite samples is not as severe as in GO.

4. Discussion

Natural graphite is a highly crystalline material [2] formed through a range of complex geological processes which can result in a wide variety of morphologies. However, flake natural graphite is predominantly formed during the creation of metamorphosed siliceous or calcareous sediments [35]. A recent extensive investigation on natural flake graphite, very

similar to the materials under consideration in this study, concluded that the flakes are comprised of polygonized stacks of interlinked crystals as seen from an angle in Figure 1A. [36]. The morphology is the result of complex crystal growth phenomena during flake formation. Disclinations and elastic instabilities lead to crystal growth along macrospirals which interlink the entire structure whilst polygonized blocks develop independently [37]. The dominant flaw in this structure is a type of prismatic edge dislocation which is better described as a region of slip misalignment. This represents a discontinuity in the crystal structure and is a very likely the point of attack for oxidants. This discontinuous layered stacking is clearly visible in Figure 8.

Consider now what may happen during the manufacture of expandable graphite. As the oxidant molecules penetrate such a flaw, the entire plane on both sides of the flaw may become heavily oxidized, to the point of resembling "graphite oxide". This is due the similar levels of oxidant concentrations used to produce intercalated graphite and "graphite oxide" [4]. This is confirmed by the very high oxygen to carbon ratio measured for the intercalated graphite materials. It is also likely that this degradation will lead to weakening of the adjacent layers, leading to further attack in the regions adjacent to these flaws. This will lead to regions of highly oxidized "graphite oxide" sandwiched between regions of relatively pristine crystallinity. The presence of considerable regions of homogenously intercalated graphite is demonstrated by the XRD traces in Figure 6. DRD reflections consistent with both graphite oxide and sulfuric acid intercalated phases are found. The oxygen to carbon ratio for "graphite oxide" may be as high as 1:1 [4]. The values for the expandable graphite grades were not as high because of the presence of regions where the graphite was not oxidized. The postulated progression of oxidation and intercalation is shown schematically in Figure 9. It is important to note that regions of overarching connectivity still exist, linking the entire flake together.

Graphite oxide is thermally unstable. It deflagrates at above 200 °C with the formation of carbon monoxide, carbon dioxide, water, and an amorphous, soot-like carbon [10, 38]. It is therefore plausible that the graphite oxide phase participates in the exfoliation of EG. Upon heating the regions of "graphite oxide" vaporize, producing large amounts of localized trapped gas. These gas pockets expand within the interlinked flake structures leading to the accordion like structures visible in Figure 2D. When the flake edges of the exfoliated graphite are examined, sheets with thicknesses exceeding those expected from the BET are also observed (Figures 2F). In Figure 8 the flaws where oxidation and intercalation may proceed are indicated by white arrows whilst the regions of overarching connectivity are indicated by red arrows.

The ash content of the two expandable graphite grades is the same and so is the oxygen to sulfur ratio. There are, however two clear differences that could hold a key to the higher thermal stability of the ES170 A300 when compared to the ES250 B5. The sulfur content of the former is lower and it contains significantly less transition metal impurities, i.e. iron and manganese. It is possible that the catalytic activity of the latter may be responsible for the lower thermal stability.

5. Conclusions

Two commercial expandable graphite (EG) samples and natural flake graphite were characterized. These expandable graphite samples were fabricated by treating natural graphite flakes with oxidants such as nitric acid and potassium permanganate in the presence of sulfuric acid. Elemental analysis revealed that the low onset temperature EG and the high temperature onset EG contained 3.03 wt.% and 2.27 wt.% sulfur respectively. The expansion onset temperatures were determined by thermomechanical analysis. They were ca. 225 °C and 300 °C respectively. Both samples released a mixture of carbon dioxide, carbon

monoxide and sulfur dioxide during exfoliation. The composition of this gas and the elemental analysis results indicate that the two samples contained more than twice the amount of oxygen expected if the EG samples were true graphite intercalation compounds with sulfuric acid units as guest ions or molecules. However, exhaustive ion exchange with diammonium phosphate confirmed that most of the sulfate ions were exchangeable. The present results are consistent with a model that assumes that the expandable graphite flakes contain both crystalline and disordered regions. The former comprise graphite layers randomly interstratified with a sulfuric acid intercalated graphite layers while the latter can be described as a graphite oxide like phase. Evidence for the presence of the graphite oxide phase comes from the broad amorphous XRD reflection consistent with a d-spacing values near 0.60 – 0.65 nm; the high oxygen content of the expandable graphite revealed by elemental analysis and the high oxygen to sulfur as well as carbon to sulfur ratios found for the evolved gases; and the transformation from a state of higher disorder to a more ordered sate on exfoliation indicated by the Raman spectra. Upon rapid heating, the oxygen-containing functional groups of the graphite oxide phase also degrade and volatilize as carbon dioxide or carbon monoxide. This explains the high oxygen to sulfur ratio of the extruded gas. Only part of the sulfur originally present is released as sulfur dioxide in the blowing gas. Some may be retained as inorganic sulfides but most probably serve to nullify dangling carbon bonds at defects and graphene edges.

Acknowledgements

This work is based upon research supported by the South African Research Chairs Initiative of the Department of Science and Technology (DST) and the National Research Foundation (NRF). Any opinion, findings and conclusions or recommendations expressed in this material

are those of the authors and therefore the NRF ad DST do not accept any liability with regard thereto.

Acknowledgements

This work is based upon research supported by the South African Research Chairs Initiative of the Department of Science and Technology (DST) and the National Research Foundation (NRF). Any opinion, findings and conclusions or recommendations expressed in this material are those of the authors and therefore the NRF ad DST do not accept any liability with regard thereto.

References

[1] D.D.L. Chung, Review: Graphite, Journal of Materials Science, 37 (2002) 1475-1489.
[2] M. Wissler, Graphite and carbon powders for electrochemical applications, Journal of Power Sources, 156 (2006) 142-150.
[3] W.S. Hummers Jr, R.E. Offeman, Preparation of graphitic oxide, Journal of the American Chemical Society, 80 (1958) 1339.
[4] C.K. Chua, Z. Sofer, M. Pumera, Graphite oxides: Effects of permanganate and chlorate oxidants on the oxygen composition, Chemistry - A European Journal, 18 (2012) 13453-13459.
[5] D.R. Dreyer, S. Park, C.W. Bielawski, R.S. Ruoff, The chemistry of graphene oxide, Chemical Society Reviews, 39 (2010) 228-240.
[6] M. Mermoux, Y. Chabre, Formation of graphite oxide, Synthetic Metals, 34 (1989) 157-162.
[7] T. Nakajima, A. Mabuchi, R. Hagiwara, A new structure model of graphite oxide, Carbon, 26 (1988) 357-361.
[8] M.S. Dresselhaus, G. Dresselhaus, INTERCALATION COMPOUNDS OF GRAPHITE, Advances in Physics, 30 (1981) 139-326.
[9] M. Inagaki, On the formation and decomposition of graphite-bisulfate, Carbon, 4 (1966) 137-141.
[10] W. Rüdorff, Graphite Intercalation Compounds, in, 1959, pp. 223-266.
[11] V.S. Leshin, N.E. Sorokina, V.V. Avdeev, Electrochemical synthesis and thermal properties of graphite bisulfate, Inorganic Materials, 40 (2004) 649-655.
[12] N.E. Sorokina, M.A. Khaskov, V.V. Avdeev, I.V. Nikol'skaya, Reaction of graphite with sulfuric acid in the presence of KMnO4, Russian Journal of General Chemistry, 75 (2005) 162-168.
[13] G. Hennig, The properties of the interstitial compounds of graphite. I. The electronic structure of graphite bisulfate, The Journal of Chemical Physics, 19 (1951) 922-929.

[14] N.E. Sorokina, O.N. Shornikova, V.V. Avdeev, Stability limits of graphite intercalation compounds in the systems graphite-HNO 3(H 2SO 4)-H 2O-KMnO 4, Inorganic Materials, 43 (2007) 822-826.
[15] G. Camino, S. Duquesne, R. Delobel, B. Eling, C. Lindsay, T. Roels, Mechanism of Expandable Graphite Fire Retardant Action in Polyurethanes, in: Fire and Polymers, American Chemical Society, 2001, pp. 90-109.
[16] V.S. Talanov, A.V. Melezhik, A.A. Chuiko, X-ray photoelectron study of the surface of expanded and expandable graphite, Theoretical and Experimental Chemistry, 28 (1993) 273-276.
[17] D.D.L. Chung, Exfoliation of graphite, Journal of Materials Science, 22 (1987) 4190-4198.
[18] E.D. Weil, S.V. Levchik, Flame retardants in commercial use or development for polyolefins, Journal of Fire Sciences, 26 (2008) 5-43.
[19] E.D. Weil, Fire-protective and flame-retardant coatings - A state-of-the-art review, Journal of Fire Sciences, 29 (2011) 259-296.
[20] L. Chen, Y.Z. Wang, A review on flame retardant technology in China. Part I: Development of flame retardants, Polymers for Advanced Technologies, 21 (2010) 1-26.
[21] Y. Nakagawa, Recent development of flame retardant polymeric materials containing expandable graphite, Bulletin of Japan Association for Fire Science and Engineering, 56 (2006) 37-43.
[22] B. Schartel, U. Braun, U. Schwarz, S. Reinemann, Fire retardancy of polypropylene/flax blends, Polymer, 44 (2003) 6241-6250.
[23] H. Seefeldt, U. Braun, M.H. Wagner, Residue stabilization in the fire retardancy of wood-plastic composites: Combination of ammonium polyphosphate, expandable graphite, and red phosphorus, Macromolecular Chemistry and Physics, 213 (2012) 2370-2377.
[24] B. Qu, R. Xie, Intumescent char structures and flame-retardant mechanism of expandable graphite-based halogen-free flame-retardant linear low density polyethylene blends, Polymer International, 52 (2003) 1415-1422.
[25] W. Zheng, X. Lu, S.C. Wong, Electrical and mechanical properties of expanded graphite-reinforced high-density polyethylene, Journal of Applied Polymer Science, 91 (2004) 2781-2788.
[26] B. Mortazavi, F. Hassouna, A. Laachachi, A. Rajabpour, S. Ahzi, D. Chapron, V. Toniazzo, D. Ruch, Experimental and multiscale modeling of thermal conductivity and elastic properties of PLA/expanded graphite polymer nanocomposites, Thermochimica Acta, 552 (2013) 106-113.
[27] W. Mhike, W.W. Focke, Surface resistivity and mechanical properties of rotationally molded polyethylene/graphite composites, Journal of Vinyl and Additive Technology, 19 (2013) 258-270.
[28] W. Mhike, W.W. Focke, J.P. Mofokeng, A.S. Luyt, Thermally conductive phase-change materials for energy storage based on low-density polyethylene, soft Fischer-Tropsch wax and graphite, Thermochimica Acta, 527 (2012) 75-82.
[29] W.W. Focke, H.J. Kruger, W. Mhike, A. Taute, A. Roberson, O. Ofosu, Polyethylene flame retarded with expandable graphite and a novel intumescent additive, Journal of Applied Polymer Science, (2014) n/a-n/a.
[30] H.J.F. Kruger, W.W.; Mhike, W.; Taute, A.; Ofosu, O., Cone calorimeter study of polyethylene flame retarded with expandable graphite and intumescent fire retardant additives, (2014).
[31] A. Skoropanov, I. Bulgak, T. Kizina, G. Kurnevich, S. Alfer, L. Malei, M. Malei, Graphite bisulphates thermal analysis, Thermochimica Acta, 93 (1985) 433-434.

[32] G. Furdin, Exfoliation process and elaboration of new carbonaceous materials, Fuel, 77 (1998) 479-485.
[33] F. Tuinstra, J.L. Koenig, Roman spectrum of graphite, The Journal of Chemical Physics, 53 (1970) 1280-1281.
[34] C. Botas, P. Álvarez, C. Blanco, R. Santamaría, M. Granda, P. Ares, F. Rodríguez-Reinoso, R. Menéndez, The effect of the parent graphite on the structure of graphene oxide, Carbon, 50 (2012) 275-282.
[35] F.J. Luque, J.D. Pasteris, B. Wopenka, M. Rodas, T.F. Barrenechea, Natural fluid-deposited graphite: Mineralogical characteristics and mechanisms of formation, American Journal of Science, 298 (1998) 471-498.
[36] H. Badenhorst, Microstructure of natural graphite flakes revealed by oxidation: Limitations of XRD and Raman techniques for crystallinity estimates, Carbon, 66 (2014) 674-690.
[37] V.N. Kvasnitsa, V.G. Yatsenko, J.A. Jaszczak, Disclinations in unusual graphite crystals from anorthosites of Ukraine, The Canadian Mineralogist, 37 (1999) 951-960.
[38] A.V. Talyzin, T.s. Szabó, I. Dékány, F. Langenhorst, P.S. Sokolov, V.L. Solozhenko, Nanocarbons by High-Temperature Decomposition of Graphite Oxide at Various Pressures, The Journal of Physical Chemistry C, 113 (2009) 11279-11284.

LIST OF TABLES

Table 1: Physical properties of graphite powders

Graphite type	**D_{10}, µm**	**D_{50}, µm**	**D_{90}, µm**	**Surface area, m^2/g**	**Density, g/cm^3**
Zimbabwean graphite	37.5	112	241	3.72 ± 0.70	2.34 ± 0.01
ES 250 B5	306	517	803	n.d.	2.08 ± 0.01
ES 250 B5 (expanded)	-	-	-	22.4 ± 2.8	-
ES170 300A	313	533	807	0.66	2.23 ± 0.01
ES170 300A (expanded)	-	-	-	14.84 ± 0.14	-

Table 2: Overall composition of the gases evolved up to 600 °C in volume fractions. The atom ratios of the evolved gases are also stated.

Component	**ES250 B5**	**ES170 A300**
CO_2	0.848 ± 0.260	0.442 ± 0.008
CO	0.135 ± 0.022	0.432 ± 0.017
SO_2	0.017 ± 0.003	0.126 ± 0.005
O/S	108	12
C/S	57	7.0
O/C	1.9	1.8

Table 3. Elemental analysis of the graphite samples. Accuracy is estimated as ± 0.3 wt.%.

Composition, wt.%	C	H	S	O[1]	Ash[2]
ES 250 B5	77.4±1.9	1.02±0.09	4.0±0.7	12.3±1.6	5.3±0.2
ES 250 B5 (expanded)	86.9±3.7	0.76±0.15	3.9±0.5	2.2±3.0	6.3±0.1
ES170 300A	82.5±0.2	0.49±0.06	3.1±0.7	8.4±0.6	5.4±1.2
ES170 300A (expanded)	88.3±0.0	0.64±0.04	2.7±0.5	2.3±0.5	6.0±1.4

[1] By difference; [2] From TGA results

Table 4. XRF results with composition indicated as wt.%

Zimbabwe graphite	**SiO_2**	**TiO_2**	**Al_2O_3**	**Fe_2O_3**	**MnO**	**MgO**	**CaO**
	3.19	0.04	1.55	1.23	0.01	0.70	0.59
	Na_2O	**K_2O**	**SO_3**	**Co_3O_4**	**S**	**Rest**	
	0.05	0.20	0.05	*<0.01*	0.13	92.20	
ES250 B5	**SiO_2**	**TiO_2**	**Al_2O_3**	**Fe_2O_3**	**MnO**	**MgO**	**CaO**
	1.20	0.03	0.49	0.21	0.29	0.45	0.18
	Na_2O	**K_2O**	**SO_3**	**Co_3O_4**	**S**	**Rest**	
	0.81	0.18	7.60	0.08	*<0.01*	88.45	
ES170 300A	**SiO_2**	**TiO_2**	**Al_2O_3**	**Fe_2O_3**	**MnO**	**MgO**	**CaO**
	1.06	0.02	0.63	0.10	0.03	0.16	1.58
	Na_2O	**K_2O**	**SO_3**	**Co_3O_4**	**S**	**Rest**	
	0.48	0.07	6.06	*<0.01*	*<0.01*	89.67	

Tabel 5. XRD d-spacing values and Raman I_D/I_G ratios.

Sample	XRD d, nm	Raman I_D/I_G
Natural graphite	0.335	0.12
ES250 5B	0.347	0.20
	0.647	
ES250 Expanded	0.337	0.13
ES170 300A	0.342	0.26
	0.335	
	0.609	
ES170 Expanded	0.337	0.10

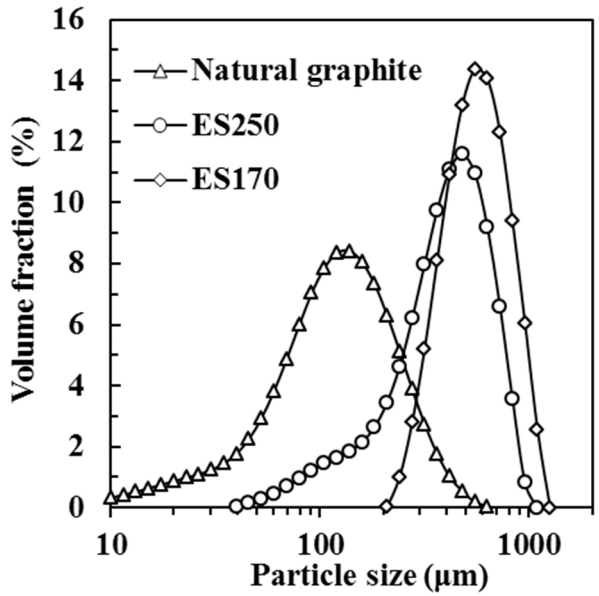

Figure 1. Particle size distribution of the various graphite samples.

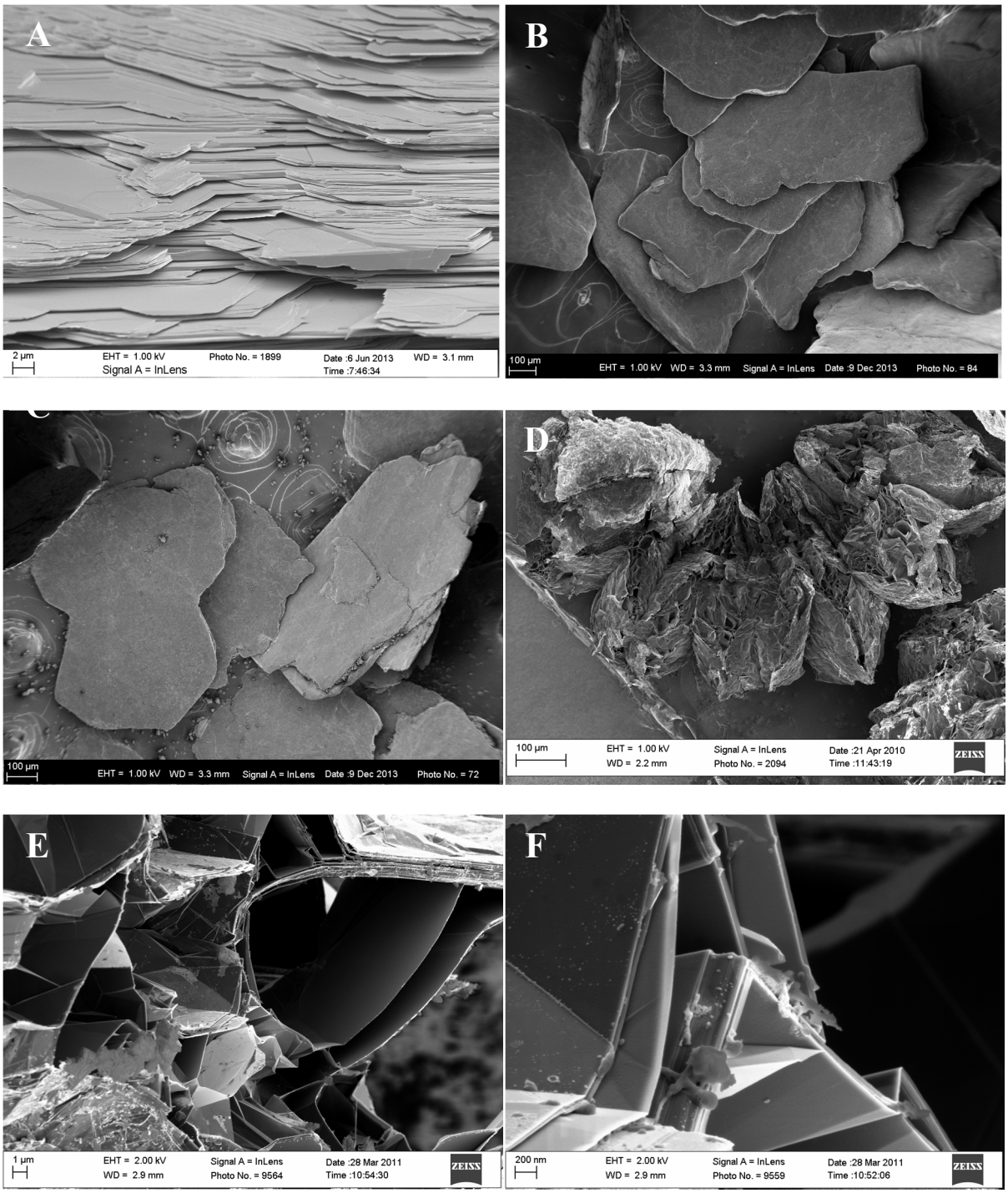

Figure 2. SEM micrographs of and graphite samples: (A) Natural Zimbabwean graphite; (B) Expandable graphite ES250 B5; (C) Expandable graphite ES170 300A; Expanded graphite ES170 300A (D) low resolution), (E) medium resolution, and (F) high resolution.

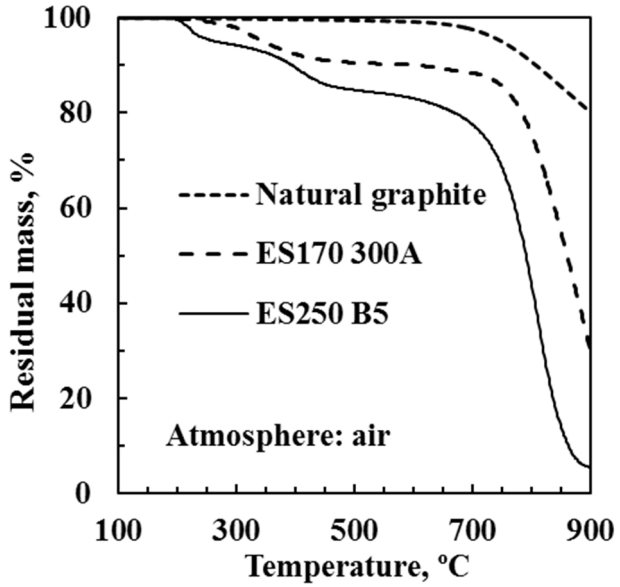

Figure 3. TGA traces in air for the three graphite samples.

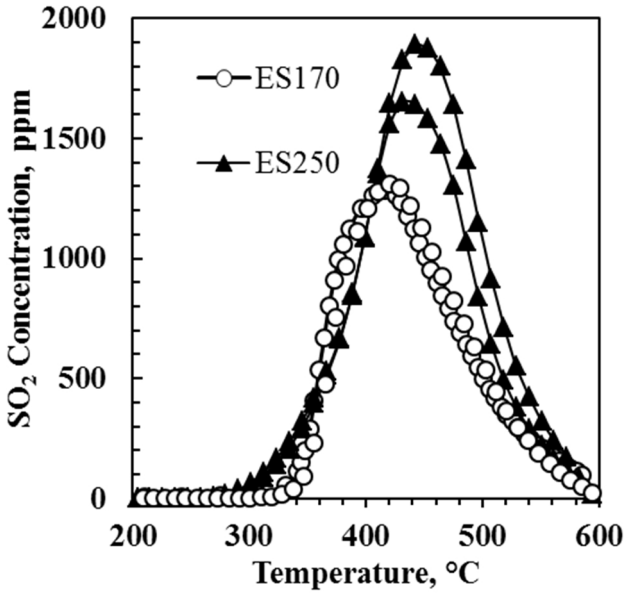

Figure 4. Sulfur dioxide release as a function of temperature for the two expandable graphite samples.

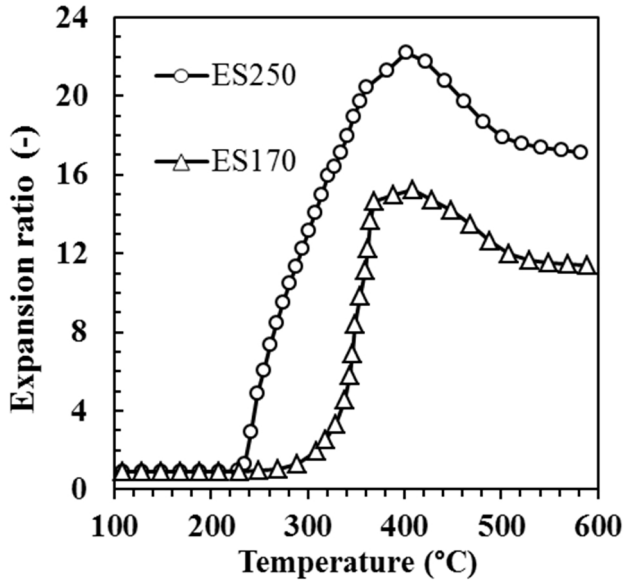

Figure 5. Thermomechanical characterization of the exfoliation process in the two expandable graphite samples.

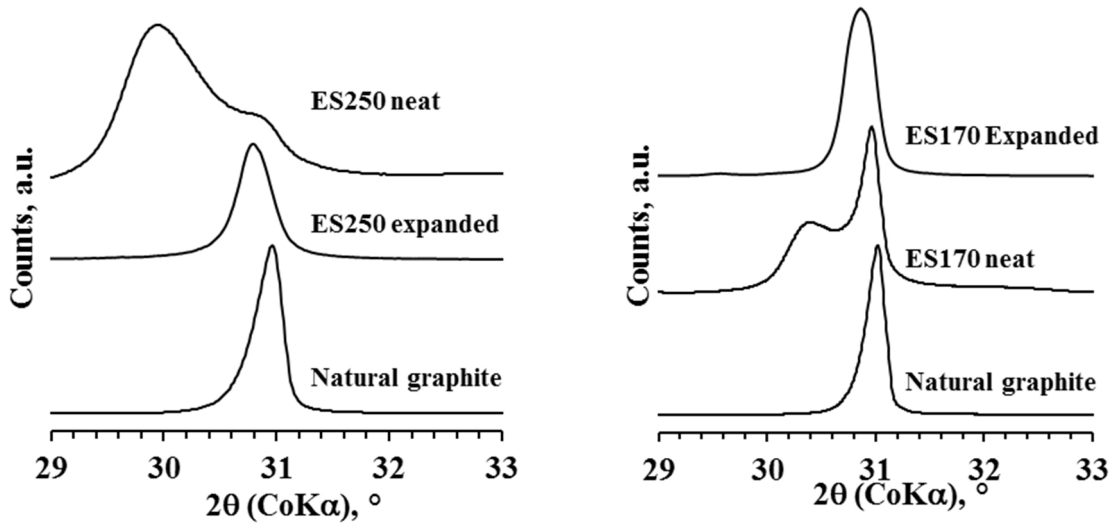

Figure 6. XRD patterns for the various states (neat and exfoliated) of the graphite samples compared to natural Zimbabwe graphite.

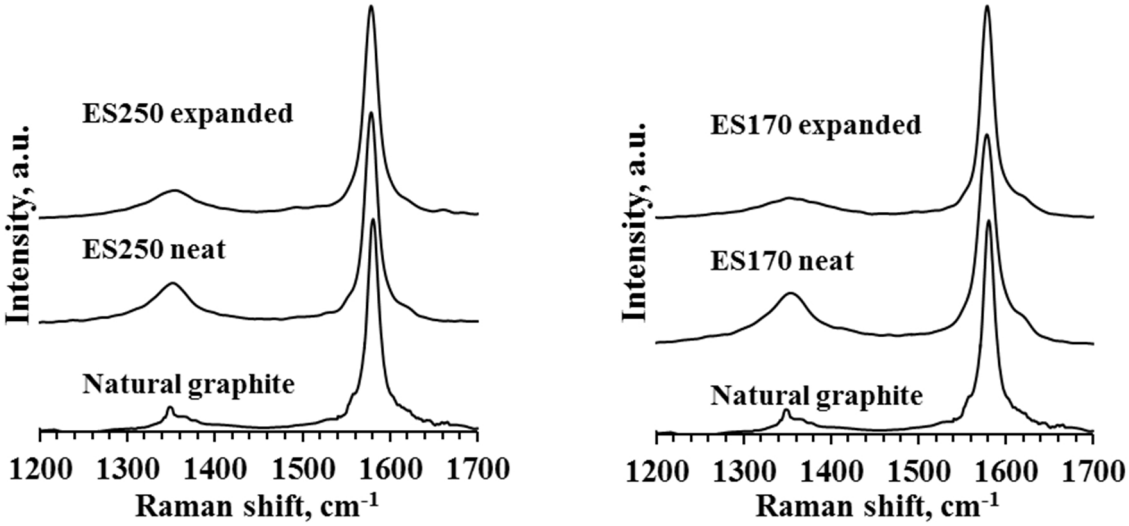

Figure 7. Raman spectra for the various states (neat and exfoliated) of the graphite samples compared to natural Zimbabwe graphite.

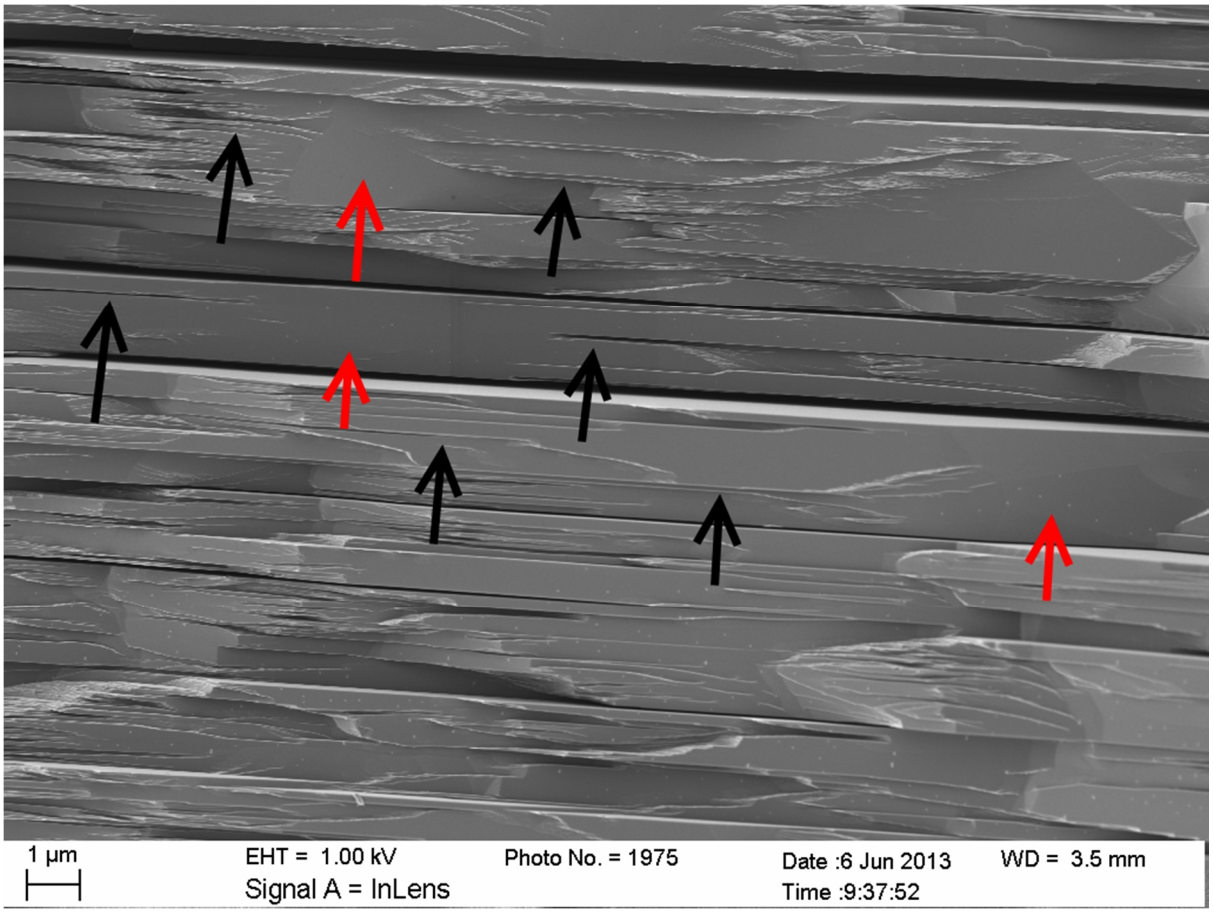

Figure 8. An edge view of a natural graphite flake. The flaws where oxidation and intercalation may commence are indicated by the white arrows while the regions of overarching connectivity are present by the red arrows.

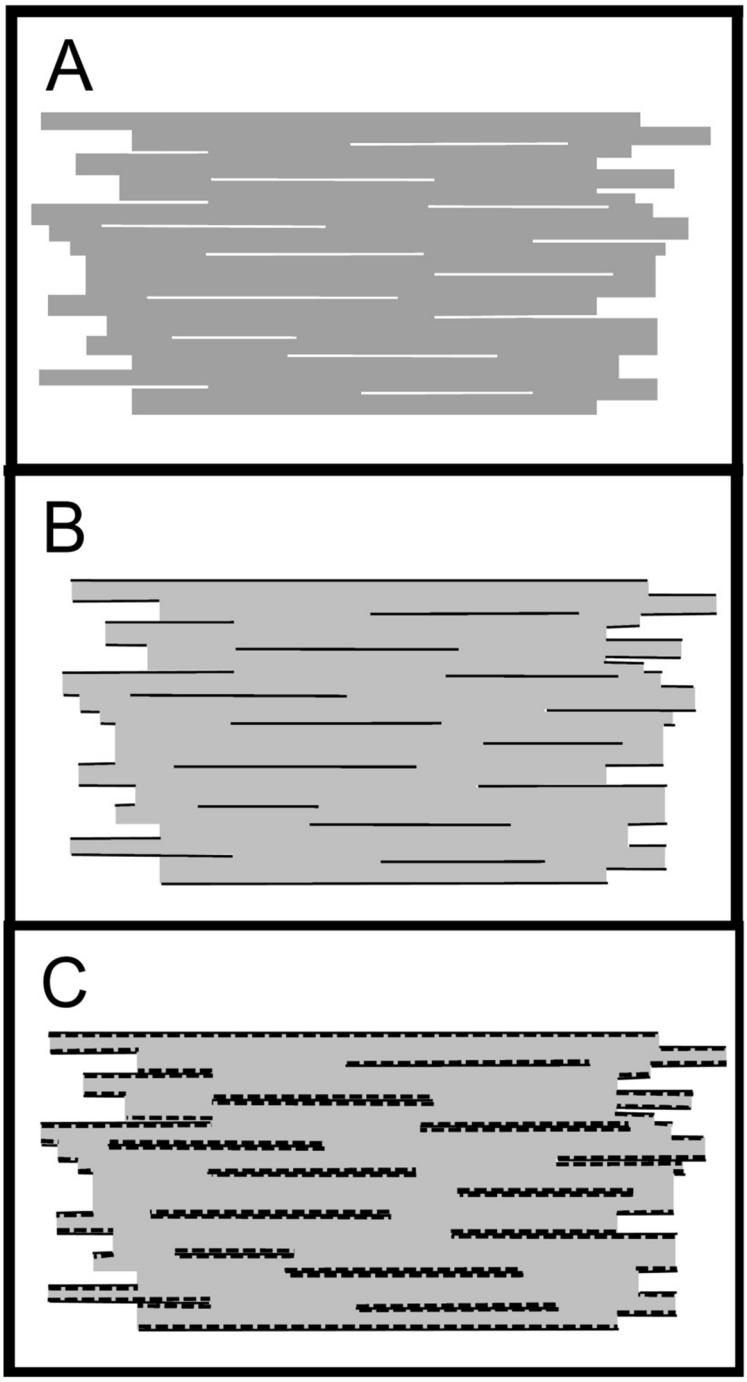

Figure 9. Postulated progression of oxidation and intercalation in natural graphite flakes. A. Neat flake showing flaws. B. Flaws provide internal access and facilitate intercalation. C. the flaws also provide easy access to water and more oxidant so that they also facilitate the conversion to graphite oxide at internal sites.